Journal of Materials Science & Technology 70 (2021) 73–82

Contents lists available at ScienceDirect

Journal of Materials Science & Technology

journal homepage: www.jmst.org

Research Article

Microstructure evolution and hot deformation behavior of carbon nanotube reinforced 2009Al composite with bimodal grain structure

K. Ma [a,b], Z.Y. Liu [a,*], S. Bi [a,b], X.X. Zhang [a], B.L. Xiao [a,*], Z.Y. Ma [a,c]

[a] Shi-changxu Innovation Center for Advanced Materials, Institute of Metal Research, Chinese Academy of Science, Shenyang, 110016, China
[b] School of Materials Science and Engineering, University of Science and Technology of China, 72 Wenhua Road, Shenyang, 110016, China
[c] School of Materials Science and Engineering, Guilin University of Technology, Guilin, 541004, China

ARTICLE INFO

Article history:
Received 10 June 2020
Received in revised form 4 July 2020
Accepted 23 July 2020
Available online 9 September 2020

Keywords:
Carbon nanotube
Bimodal
Aluminum matrix composite
Hot deformation
Processing map

ABSTRACT

The hot deformation behaviors of the bimodal carbon nanotube reinforced 2009Al (CNT/2009Al) composite were studied by establishing processing map and characterizing the microstructure evolution. The results indicate that the grain size in the ultra-fine grained zones was stable during hot deformation, while the coarse grained zones were elongated with their long axis directions tending to be perpendicular to the compression direction. Low temperature with high strain rate (LTHR), as well as high temperature with low strain rate (HTLR) could increase the length/width ratio of the coarse grained zones. However, LTHR and HTLR could cause the instable deformation. The instable deformation at LTHR was induced by severe intragranular plastic deformation and the localized shear crack, while the instable deformation at HTLR resulted from the more deformation component at the coarse grained zones, and the micro-pore initiation due to CNT re-agglomeration at the boundaries between the coarse and the ultra-fine grained zones.

1. Introduction

Carbon nanotubes (CNTs) have attracted much attention as the ideal reinforcements for aluminum matrix composites due to their extremely high elastic modulus (~1 T Pa), high strength (>30 GPa) as well as good thermal and electrical properties [1–3]. Lots of studies have shown that the strength and modulus of the CNT/Al composites could be enhanced compared with those of the matrixes [4–10]. However, the CNT/Al composites have a significant drawback of low ductility, restricting their industrial application. One of the main reasons for their low ductility is the extensively refined grain size caused by the strong pinning effect of CNTs on grain boundaries (GBs) [5,11–14].

Recently, the bimodal structure design with inhomogeneous distribution of reinforcements or grain sizes was demonstrated to be a potentially effective way of improving the strength-ductility of CNT/Al and other ultra-fine grained composites [15–18]. For example, Liu et al. [17] fabricated the bimodal CNT/Al-Cu-Mg composite by introducing CNT-free coarse grained zones into CNT-rich ultra-fine grained zones, and achieved more than twice the elongation with nearly no ultimate tensile strength loss as compared to the uniform CNT/Al-Cu-Mg composite. The enhanced elongation was attributed to the greatly suppressed strain localization and effectively blunted micro-cracks due to the inhomogeneous structure. Meanwhile, geometrically necessary dislocations were induced between the coarse and ultra-fine grains, leading to extra-strengthening beyond the rule-of-mixtures.

In general, for aluminum matrix composites, especially the CNT/Al composites, large hot-deformation, e.g. extrusion or rolling, is required to achieve good mechanical properties [19–22]. However, the large difference of the mechanical properties between the different zones in the bimodal materials would lead to inhomogeneous flowability during hot deformation, which could greatly deteriorate the material deformability [23]. For example, Raja et al. [24] investigated the superplastic behavior of AZ91 magnesium alloy with mixed grain size, and found that the material exhibited a much lower elongation than the fine-grained material at high temperature, attributable to the strain localization promoted by the inhomogeneous structure. Nevertheless, the formability of inhomogeneous materials could be improved by optimizing the deformation parameters. For example, Pradeep et al. [25] obtained the superplasticity of layered 5086Al alloy with inhomogeneous grains. The deformation coordination of the different zones was effectively improved by optimizing the deformation temperature

* Corresponding authors.
E-mail addresses: zyliu@imr.ac.cn (Z.Y. Liu), blxiao@imr.ac.cn (B.L. Xiao).

https://doi.org/10.1016/j.jmst.2020.09.003

and strain rate. Therefore, in order to avoid the instable deformation and improve the formability of bimodal CNT/Al composites, it is necessary to investigate the hot deformation behaviors.

Furthermore, the strength-ductility of the bimodal CNT/Al composites was significantly influenced by the inhomogeneous structure parameters. Liu et al. [17] found that there were a lower limit concentration and an optimized width of coarse grain for achieving bimodal CNT/Al composites with high strength-ductility. So far, there were no studies on the evolution of bimodal structure in the hot deformation of CNT/Al composites. However, it was reported that hot deformation had a significant effect on the evolution of the bimodal structure for other materials [24,26]. For example, Xu et al. [26] characterized the microstructure of bimodal Al-7.5 Mg alloy after hot extrusion, and found the coarse grains were elongated along the extrusion direction, the ultra-fine grains maintained equiaxed shape.

Under some in-approximate conditions, the bimodal structure could even disappear after hot deformation. For example, Liu et al. [27] found that the bimodal structure of Udimet 720Li superalloy was completely destroyed during hot deformation. The grain size of coarse grain zones was continuously refined due to dynamic recrystallization (DRX), while the grain growth occurred in the fine grain zones. Unlike that in unreinforced alloys, there were a large number of CNTs in the ultra-fine grained zones of the bimodal CNT/Al composite, and CNTs had strong pinning effect on the GBs [17,28]. Therefore, the microstructure evolution of bimodal CNT/Al composites might be quite different. In order to realize the controllable microstructure and optimize the properties, it is necessary to study the microstructure evolution in different zones of bimodal CNT/Al composites.

In this study, a bimodal CNT/2009Al composite was fabricated by a combination of ball milling and powder metallurgy processing, and the processing maps were established based on hot compression tests. The microstructure evolution and flow instable behavior were analyzed. The aim is to (a) obtain a parameter range suitable for hot working, (b) establish the relationship between processing parameters and microstructures, and (c) clarify the mechanism of deformation instability for this bimodal CNT/2009Al composite.

2. Experimental details

2.0 wt.% CNTs fabricated by chemical vapor deposition in Tsinghua University (Fig. 1(a)), with an average diameter of 15 nm and an average length of 5 μm were mixed with 2009Al alloy (Al-4.5 wt.% Cu-1.5 wt.% Mg) powders with an average diameter of 10 μm (Fig. 1(b)) in a mixer for 6 h. Then, the as-mixed powders were ball milled for 10 h in an attritor at a rotational speed of 250 rpm with a ball powder ratio of 15:1. No extra pre-treatment was conducted on CNTs. 2.0 wt.% stearic acid was added to prevent serious cold-welding. The morphologies of the milled CNT/2009Al powders are shown in Fig. 1(c). The as-milled CNT/2009Al powders had a smaller powder size and an irregular morphology. The as-milled powders were mechanically mixed with 25 wt.% 2009Al alloy powders with an average diameter of 10 μm for 6 h. Then the as-mixed powders were cold-compacted in a cylinder die, degassed and finally hot pressed at 560 °C for 1.5 h into cylindrical billets. Cylindrical specimens with a diameter of 8 mm and a height of 12 mm in concordance with ASTM E9-09 standard were machined from the hot-pressed billets, with the compression axis parallel to the hot pressed direction.

Isothermal compression tests were conducted at temperatures of 300, 350, 400, 450, and 500 °C with strain rates of 0.001, 0.01, 0.1, 1 s^{-1} on a Gleeble-3800 thermal-simulator system. Graphite sheets were used to lubricate both end surfaces of the specimens. The specimens were rapidly heated to the test temperature at a heating rate of 10 °C/s and then held for 10 min to eliminate the thermal gradient. Then the specimens were compressed to a true strain of 0.8 at the set strain rate. The true strain-true stress curves were automatically recorded during the hot compression process. After hot compression, the specimens were quickly quenched into the water to freeze the microstructure. The specimens were cut through the centerline along the compression direction for microstructure examinations.

The samples were mechanically polished and etched using the Graff and Sargent's reagent, then observed by optical microscopy (OM; Zeiss Axiovert 200 MAT), scanning electron microscopy (SEM; FEI Quanta600). Transmission electron microscopy (TEM; Tecnai G2 20) was applied to characterize the grains and CNT distribution. TEM specimens were cut by electrical discharge machining, ground to a thickness of 60 μm, punched to disks with a diameter of 3 mm, then dimpled to a minimum thickness of 20 μm and finally ion-beam thinned by a Gatan Model 691 ion milling system.

Electron backscattered diffraction (EBSD; Zeiss Supra 55) was used to observe the grain structure of the coarse grained zones. The grain type was determined by the grain orientation spread (GOS) value associated with the dislocation densities [29]. For a deformed grain, the dislocation density is high and dislocations are arranged in substructures, this results in local misorientations of several degrees within grains and the GOS value is high [30]. For a recrystallized grain, the dislocation density is low, thus the misorientation degrees within grains were extremely low and the GOS value is low. In the present study, the grains with GOS value of <2°, 2°–5° and >5° were respectively considered as recrystallized grain, sub-structure grain and deformed grain [29].

3. Results

3.1. Initial microstructural

The microstructures of the as hot-pressed CNT/2009Al composite are shown in Fig. 2. It can be seen that the coarse grained zones were uniformly embedded in the ultra-fine grained zones. According to the measurement and statistical analysis, the average diameter of the coarse grained zones was about 7 μm, and the content of the coarse grained zone was about 25.6 vol.% which was nearly equal to the concentration of the additional un-milled 2009Al powders. Some undissolved phases were mainly distributed in the ultra-fine grained zones. The energy dispersive spectrometer (Fig. 2(b)) indicates that the undissolved phase was rich in Cu and Mg, which was a common phase in 2xxx Al alloys. CNT distribution shown in Fig. 2(c) demonstrates that a large number of CNTs were uniformly and singly distributed in the ultra-fine grained zones, while no CNTs were found in the coarse grained zones. The grain structure shown in Fig. 2(d) indicates that the ultra-fine grains were of equiaxed shape, after counting 200 ultra-fine grains, the average grain size was obtained with about 200 nm. These results indicate that the CNT/2009Al composite with a bimodal structure was successfully obtained.

3.2. True stress-true strain curves

Fig. 3 shows the typical true stress-true strain curves of the bimodal CNT/2009Al composite specimens compressed at 450 °C and strain rate of 1 s^{-1}, respectively. At 450 °C, the flow stress increased with increasing the strain rate (Fig. 3(a)). Further, the curves exhibit evident peak stress at the initial deformation stage except for that at a strain rate of 0.001 s^{-1} (Fig. 3(a)). It is believed that the dislocations accumulated at the initial stage of deformation increased the flow stress, then the flow stress decreased as dislocations quickly reacted with each other or annihilated at the

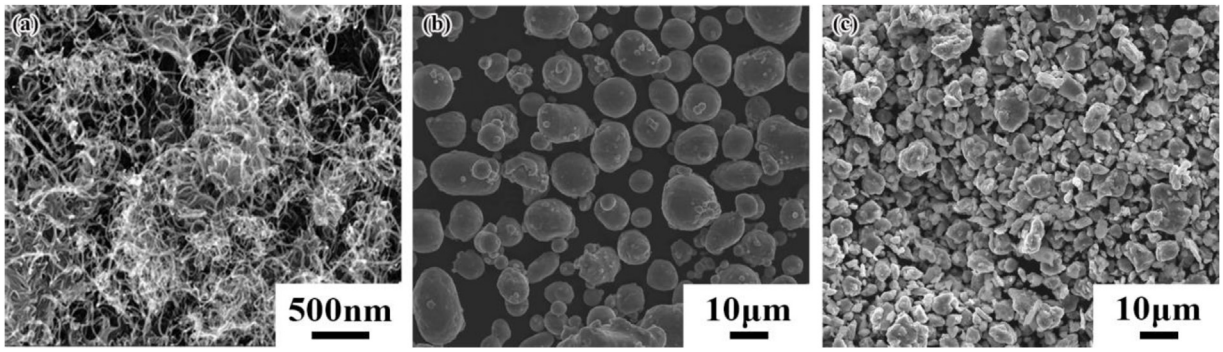

Fig. 1. Powder morphologies of (a) the raw CNTs, (b) the raw 2009Al alloy, (c) the ball-milled CNT/2009Al.

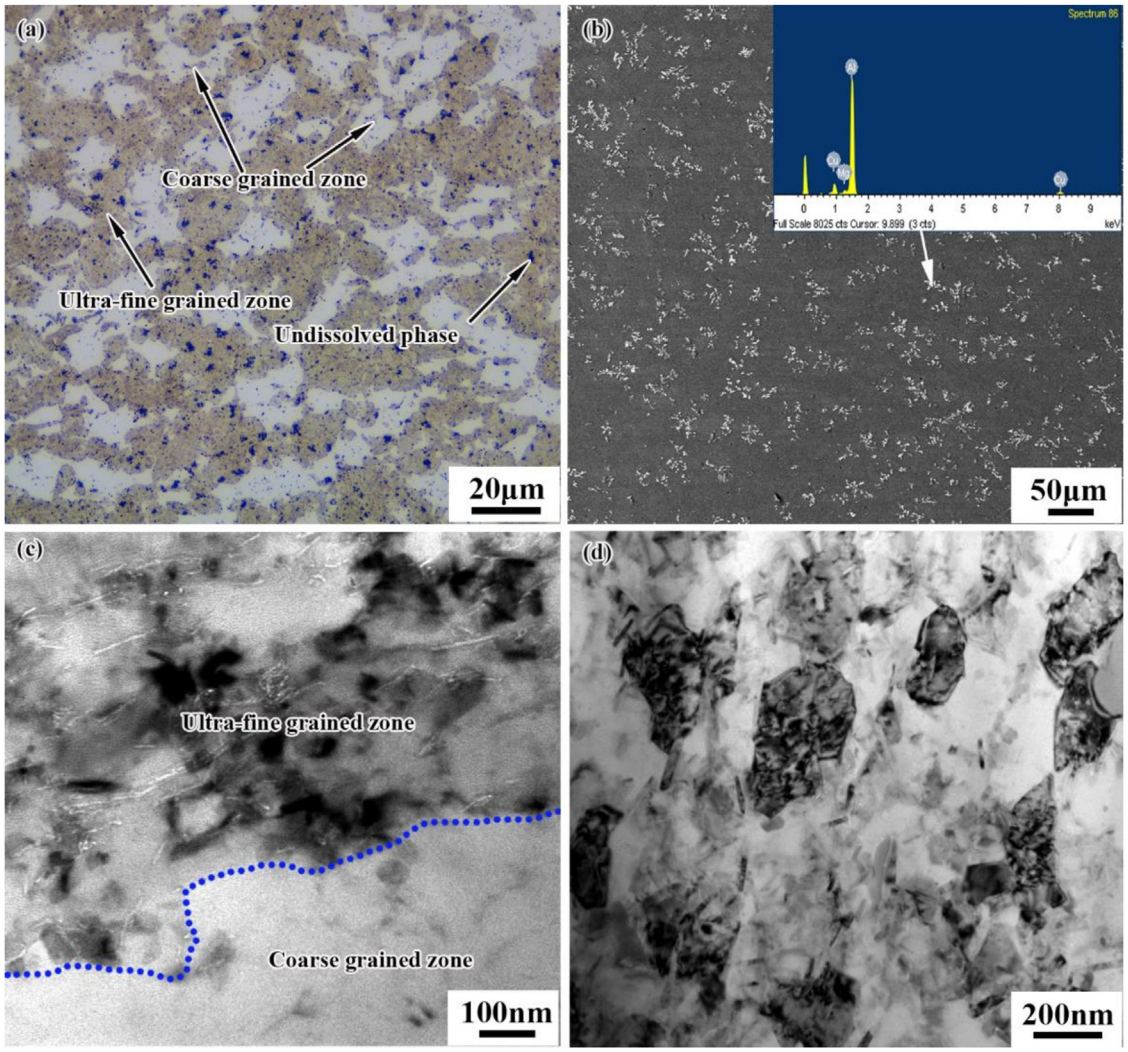

Fig. 2. Initial microstructures of as hot-pressed CNT/2009Al composite: (a) OM image of macrostructure, (b) SEM back-scattered electron image and EDS of undissolved phases, (c) TEM image of CNT distribution, and (d) TEM image of grain structure in ultra-fine grain zones.

GBs with increasing the strain [31,32]. For the composite specimen compressed at the low strain rate of 0.001 s^{-1}, the dislocations accumulated slowly and had sufficient time to react or annihilate, then the hardening and softening of the stress would reach equilibrium at the initial stage of deformation. At the strain rate of 1 s^{-1}, the flow stress decreased gradually with increasing temperature (Fig. 3(b)). Similar phenomena have also been found in other alloys or composites [33,34]. This was due to the thermal activation of Al matrix and the enhancement of kinetic energy, which promoted the dislocation movement at elevated temperature [35].

3.3. Processing maps

Processing maps are an effective alternative to investigate hot deformation behaviors [29,36–38]. Among them, different microstructure evolutions correspond to different power dissipation efficiency (η), and the safe window of processing parameters

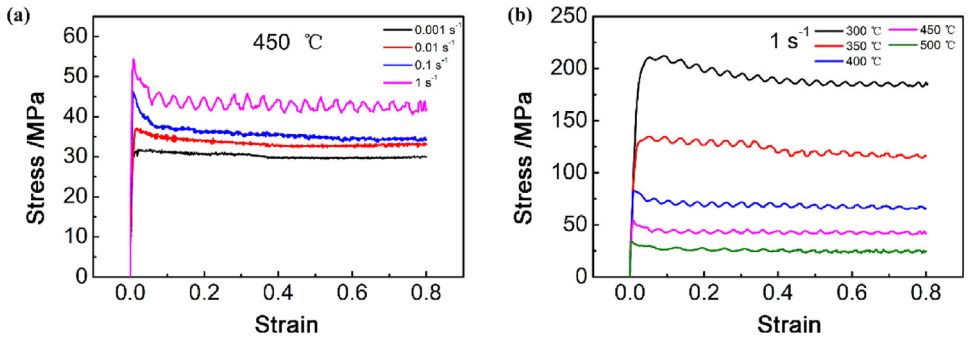

Fig. 3. Compressive true stress-true strain curves of bimodal CNT/2009Al composite specimens at (a) 450 °C with different strain rates; (b) 1 s^{-1} with different temperatures.

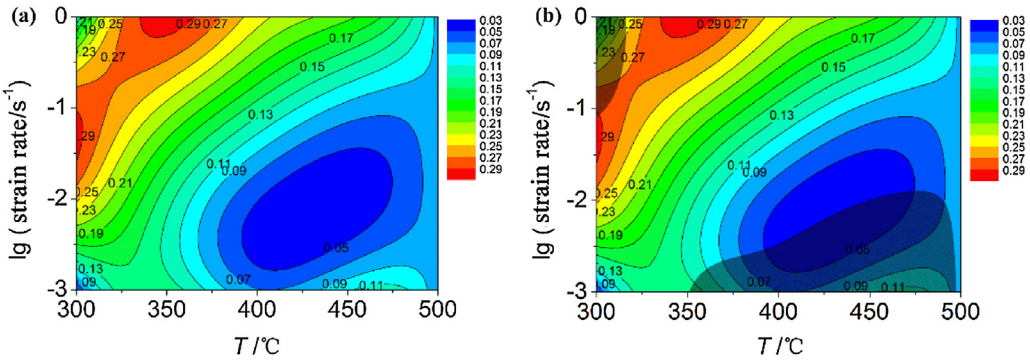

Fig. 4. Processing maps of bimodal CNT/2009Al composite: (a) power dissipation map; (b) processing map containing instable zone.

can be obtained by defining the instable zone. The η of the bimodal CNT/2009Al composite deformed at a true strain of 0.8 under different parameters was calculated based on Murty model [39], and the results are shown in Fig. 4(a). The instable zone was determined using the Prasad model [40], as shown by the shaded area in Fig. 4(b). Two instable zones could be observed. One was the deformation zone of low temperature with a high strain rate (LTHR), and the other was the deformation zone of high temperature with a low strain rate (HTLR).

The η map and instable zone for the bimodal CNT/2009Al composite were quite different from those of uniform CNT/Al composites [29,36,41]. It has been reported that the η of the uniform CNT/Al-Cu-Mg composite increased with increasing temperature and decreasing strain rate, and it reached the highest value of 0.30 at 400 °C with 0.001 s^{-1}, because the DRX at high temperature with low strain rate was beneficial to reduce the risk of deformation damage [29].

Unlike the uniform CNT/Al composite, the present bimodal CNT/2009Al composite exhibited decreased η with increasing temperature and decreasing the strain rate, and the η was only 0.07 at 400 °C with 0.001 s^{-1}. Considering the inhomogeneous distribution of CNTs and the dual-scale grain structure in the present bimodal CNT/2009Al composite, the relationship of microstructure evolution with flowing behavior must be taken into account for the special η variation with temperature and strain rate.

3.4. Microstructure evolution

Typical OM images of the bimodal composite specimens after compression with the true strain of 0.8 at different parameters are shown in Fig. 5. The coarse grained zones were elongated and their long axis directions tended to be perpendicular to the compression direction. For simplifying, the direction perpendicular and parallel to the compression direction are respectively defined as the length direction and width direction. It can be seen the width of the coarse grained zones compressed at 450 °C with 1 s^{-1} was larger than other parameters.

In order to quantitatively analyze the evolution of the coarse grained zones, the morphology parameters of the coarse grained zones under different deformation parameters were measured by Image Tool software using a mean linear intercept method. 200 coarse grained zones were counted in each sample, and the error bars were obtained according to the standard deviation in statistics, as shown in Fig. 6. At the high strain rate of 1 s^{-1}, with the increase of deformation temperature, the length of the coarse grained zones increased firstly and then decreased (Fig. 6(a)), while the width of the coarse grained zones gradually increased (Fig. 6(c)). At 450 °C, with the increase of strain rate, the length of the coarse grained zones decreased (Fig. 6(b)) and the width of the coarse grained zones gradually increased (Fig. 6(d)). The content of the coarse grained zones at a high strain rate of 1 s^{-1} remained almost the same as that before deformation (Fig. 6(e)). However, at a high temperature of 450 °C, with decreasing the strain rate, the content of the coarse grained zones increased (Fig. 6(f)), which means the existence of abnormal grain growth (AGG) at HTLR. In summary, LTHR and HTLR could increase the length/width ratio of coarse grained zones, but HTLR could lead to increased content of coarse grained zone.

Fig. 7 shows the grain structure of the bimodal CNT/2009Al composite specimens compressed at different deformation parameters. EBSD results demonstrate that only the coarse grained zones could be resolved. At 350 °C with 1 s^{-1}, the proportion of deformed grains was as high as 55.6 %, and the proportion of recrystallized grains was very low, only 18.1 % (Fig. 7(a) and (d)). At 450 °C with 1 s^{-1}, the proportion of deformed grains was decreased to 15.6 %, and the pro-

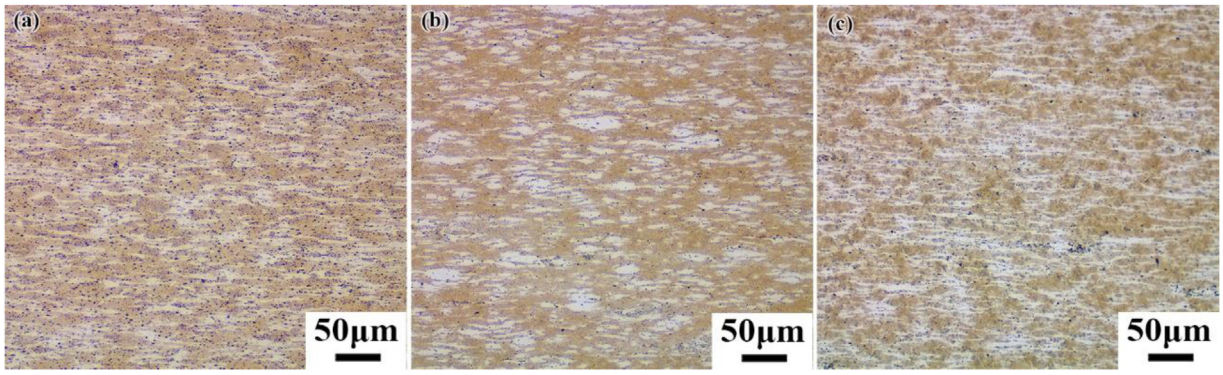

Fig. 5. OM images of bimodal CNT/2009Al composite specimens compressed to a true strain of 0.8 at (a) 300 °C with 1 s^{-1}; (b) 450 °C with 1 s^{-1} and (c) 450 °C with 0.001 s^{-1}.

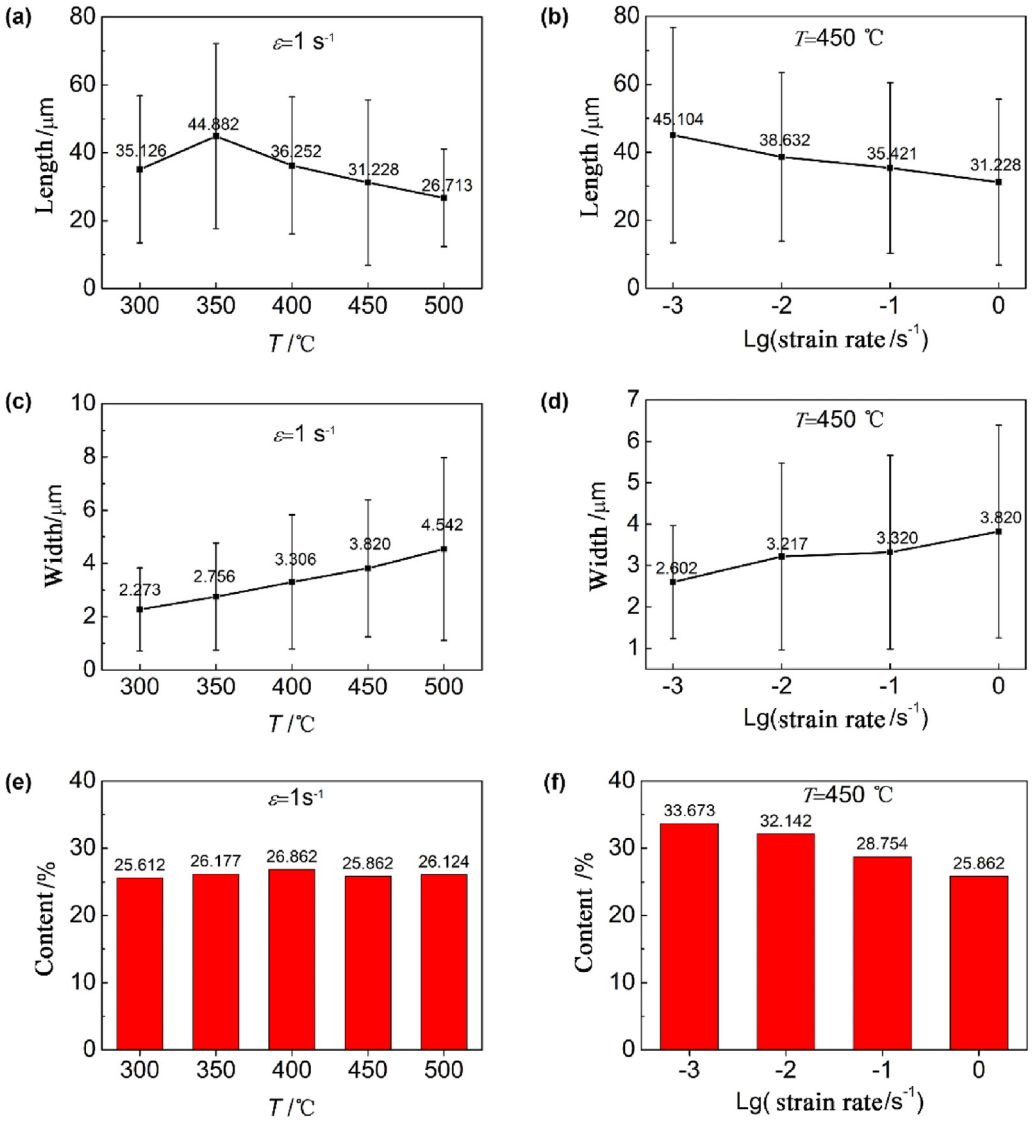

Fig. 6. The statistical results of (a), (c), (e) average length, width and content of coarse grained zones at strain of 1 s^{-1} with different temperatures; (b), (d), (f) average length, width and content of coarse grained zones at temperature of 450 °C with different strain rates.

portion of recrystallized grains was increased to 40.3 % (Fig. 7(b) and (e)). At 450 °C with 1 s^{-1}, the proportion of deformed grains further decreased to 15.1 %, and the proportion of recrystallized grains was further increased to 69.8 % (Fig. 7(c) and (f)). With increasing the deformation temperature or decreasing the strain rate, the recrystallized grain fraction of the coarse grained zones increased, while the deformed grain fraction decreased. It means that enough thermal energy and action time for the interaction and annihilation of dislocations could be provided at HTLR, and the dislocation density could be greatly reduced.

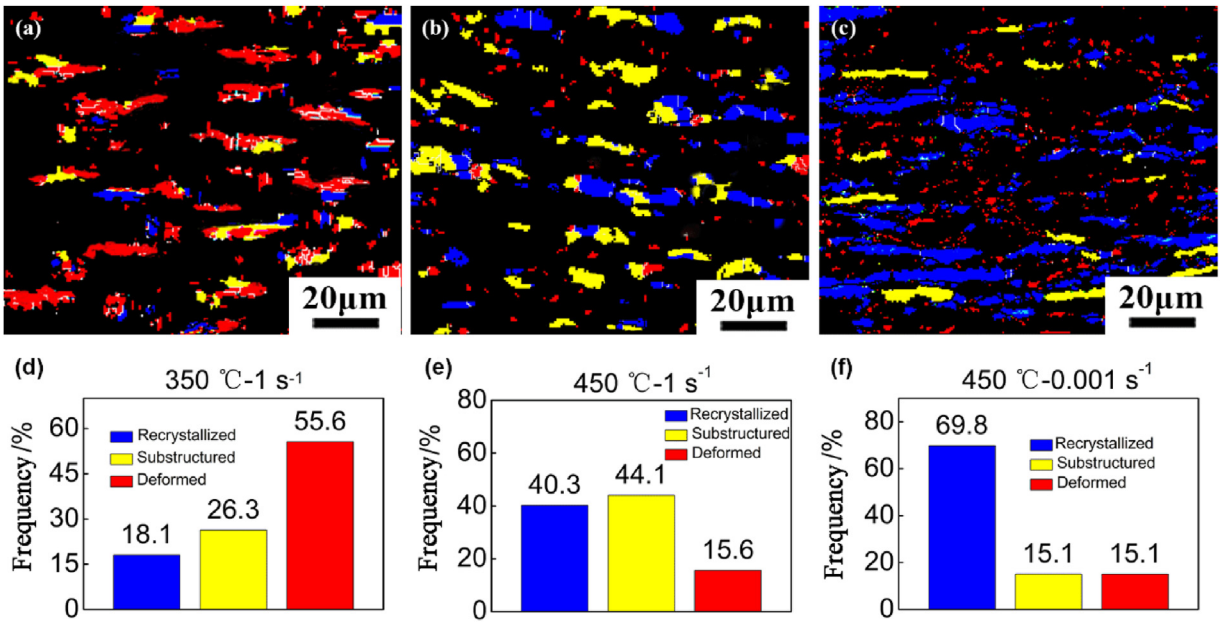

Fig. 7. Grain type distribution maps characterized by EBSD and their proportions in coarse grained zones compressed at (a), (d) 350 °C with 1 s^{-1}, (b) (e) 450 °C with 1 s^{-1}, (c) (f) 450 °C with 0.001 s^{-1}.

Fig. 8 shows the TEM images of grain structures for the bimodal CNT/2009Al composite specimens compressed at different parameters. It can be found the microstructures of the coarse grained zones under different parameters were quite different. For the specimen compressed at 350 °C with 1 s^{-1}, sub-grain boundaries were formed within the coarse grains (Fig. 8(a)), indicating the existence of continuous DRX. The newly formed sub-grain boundaries had a good ability to storage the imported power, thereby inducing a high η [37].

For the specimen compressed at 450 °C with 1 s^{-1}, a lot of tangled dislocations formed within the coarse grains (Fig. 8(c)). The tangled dislocation consumed the imported power substantially in the form of heat dissipation. Therefore, the power stored in the microstructure evolution was low, which resulted in a much lower η than that of the specimen compressed at 350 °C with 1 s^{-1}.

For the specimen compressed at 450 °C with 0.001 s^{-1}, the dislocation density in the coarse grained zone was extremely low, and clear GBs were formed within the coarse grained zones (Fig. 8(e)). It indicates the existence of DRX, which was consistent with the results of EBSD characterization (Fig. 7(e), (f)). However, the η was extremely low at this parameter. This might be related to the AGG, which agreed well with the previous investigation on SiC/2014Al composite [32]. On one hand, the content of the GBs reduced, so the power stored in the GBs decreased. On the other hand, AGG aggravated the inhomogeneous microstructure, and easily led to localized deformation. Because the effective area for power dissipation was reduced, the extremely low η was obtained.

The microstructures of the ultra-fine grained zones under different parameters were similar to each other (Fig. 8(b), (d) and (f)). All the ultra-fine grains were equiaxed, and the grain sizes at different deformation parameters were approximately the same with an average grain size of about 200 nm. This means that the pinning effect of CNTs at the GBs of the ultra-fine grains could effectively impede the GB migration, and the ultra-fine grains were difficult to coarsen [42]. Further, no dislocation walls or sub-grain boundaries were found in the ultra-fine grains, while some rod-like phase could be observed in the ultra-fine grained zone. This rod-like phase was believed to be Al_4C_3, which was a common phase for CNT/Al composites [12].

4. Discussion

4.1. Evolution mechanism of coarse grained zones

As the toughening zone in the bimodal composites, the coarse grained zone plays an important role in controlling the properties [17]. It is necessary to investigate the evolution mechanism of the coarse grained zone during hot deformation.

Figs. 5 and 6 show that both LTHR and HTLR increased the length/width ratio of the coarse grained zones. In general, dislocation cutting often caused grain refinement at LTHR [43,44]. When the coarse grained zones underwent a large compression deformation, the refined grains in the coarse grained zones would also be rearranged along the deformation direction, resulting in a significant reduction in the width of the coarse grained zones. Simultaneously, the contribution of GB sliding to plastic deformation was relatively small and the intragranular deformation was more prominent, due to the low deformation temperature. It means that the grains in the coarse grained zones were easily elongated in the direction perpendicular to the compressive stress. As a result, the coarse grained zones with a large length/width ratio were achieved.

At HTLR, the width of the coarse grained zones was small which could attribute to the inhomogeneous deformation between the coarse and ultra-fine grained zones. Generally, GB sliding of matrix alloys would become easier with the increase of deformation temperature or the decrease of strain rate [33,45]. As the temperature is constant, the shear stress required by GB sliding can be drawn as [46]:

$$\tau = \frac{Kd}{\rho}\dot{\gamma} \tag{1}$$

where τ is the shear stress required by GB sliding, K is the constant, d is the grain size, ρ is the defect density and $\dot{\gamma}$ is the shear strain rate.

For the bimodal CNT/Al composite, the CNTs pinning at the GBs would increase the difficulty for the GB sliding in the ultra-fine

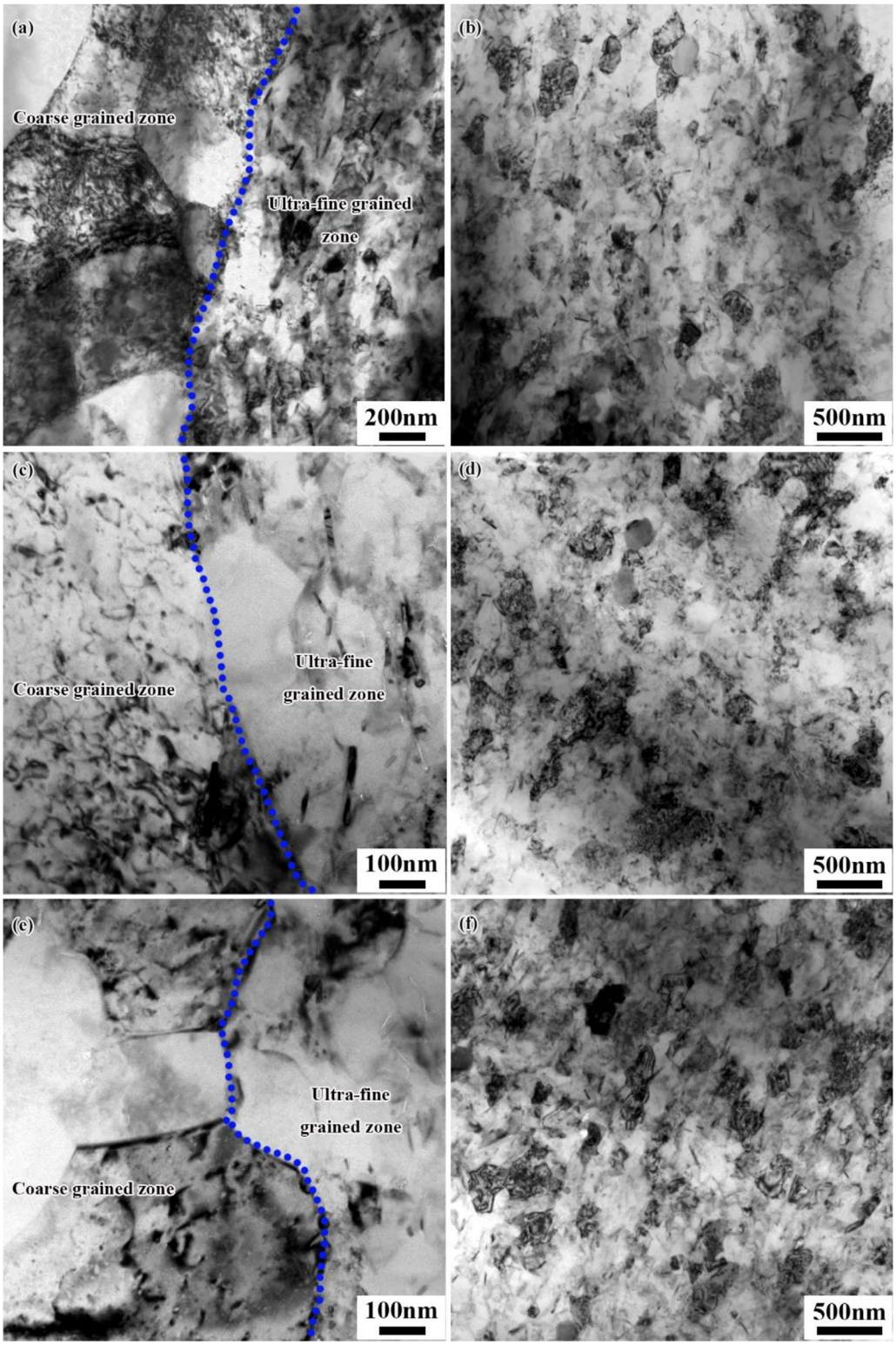

Fig. 8. TEM images of bimodal CNT/2009Al composite specimens compressed to a true strain of 0.8 at (a), (b) 350 °C with 1 s^{-1}, (c) (d) 450 °C with 1 s^{-1}, (e) (f) 450 °C with 0.001 s^{-1}.

grained zones. The drag effect of reinforcements can be expressed by the following equation [47,48]:

$$\tau_1 = \eta_I \dot{\gamma} \quad (2)$$

where τ_1 is the dragging force, η_I is the interface viscosity which can be expressed by the following equation [47]:

$$\eta_I = M\dot{\gamma}^{-p} \quad (3)$$

where both M and p are the constants as the temperature is constant. By substituting Eq. 3 into Eq. 2, the final form can be obtained as follows:

$$\tau_1 = M\dot{\gamma}^{1-p} \quad (4)$$

By comparing Eq. (4) with Eq. (1), it can be found that the decrease of the drag force is lower than that of the shear stress required by GB sliding, with decreasing the shear strain rate. The lower the strain rate was, the smaller proportion of deformation in the ultra-fine grained zone was. Therefore, the deformation was more concentrated in the CNT-free coarse grained zones at HTLR, which could lead to a large length/width ratio of the coarse grained zones at this parameter.

4.2. Deformation instability

Fig. 9 shows the damage morphology under two typical instable deformation parameters. There were pronounced differences of damage morphologies between the two instability zones. For the specimen compressed at 300 °C with 1 s^{-1}, the crack of about 30 μm in length and 5 μm in width could be observed (Fig. 9(a)). Cracking at LTHR has also been widely found in other alloys or composites [11,41,45,49]. It is mainly attributed to the localized shear deformation promoted by the intense intragranular deformation [50,51].

For the specimen compressed at 450 °C with 0.001 s^{-1}, as shown in Fig. 9(b), a large number of micropores could be found at the boundaries between the coarse and ultra-fine grained zones (BCFZ). The instable deformation mechanism needs to be further analyzed by fine microstructure observation.

Fig. 10 shows the distribution of CNTs (marked by black arrows) under two typical instable deformation parameters. It can be seen CNTs maintained good structure morphology. According to the previous characterization results of the CNTs in the CNT/Al composite after hot extrusion [12], it can be known that the structural damage of CNTs caused by hot deformation was weak. However, the distribution of CNTs would be changed with different deformation parameters. For the specimen compressed at LTHR, the CNTs near and far from the BCFZ were both uniformly distributed (Fig. 10(a) and (b)). For the specimen compressed at HTLR, the CNTs far from the BCFZ were uniformly distributed (Fig. 10(d)), but the CNTs near the BCFZ were densely distributed (Fig. 10(c)), indicating the re-agglomeration of CNTs near the BCFZ. Simultaneously, no CNTs were observed in the coarse grained zones. As previously described, AGG occurred at HTLR. Therefore, it can be deduced that AGG was not caused by the growth of ultra-fine grains, but controlled by the GB migration from the coarse grained zone to the ultra-fine grained zone, which could lead to the decrease of grain size in the ultra-fine grained zone near BCFZ until it is merged by coarse-grained zone. However, the grain size in the ultra-fine grained zone far from the BCFZ kept stable. And under the thrust of GB migration, the re-agglomeration of CNTs near the BCFZ occurred.

Obviously, the re-agglomeration of CNTs at the BCFZ would increase the stress concentration and induce micro-pore nucleation at these positions. It should be noted that, according to Eq. (4), the dragging force of CNTs at HTLR was strong and more deformation occurred in the coarse grained zones, which would further accelerate the stress concentration at the BCFZ. Based on the above two reasons, micro-pores were formed at the BCFZ under HTLR (Fig. 10(c)).

Finally, the morphology evolution of the coarse grained zones in the bimodal CNT/2009Al composite can be summarized as follow. LTHR as well as HTLR could increase the length/width ratio of the coarse grained zones. At LTHR, the large length/width ratio of the coarse grained zones could attribute to that the refined grains induced by dislocation cutting rearranged along the deformation direction. With increasing the deformation temperature, at high temperature with a high strain rate, the GB sliding became easier, leading to a reduction in the intragranular deformation, thereby reducing the length/width ratio of the coarse grained zones. At HTLR, both the coarse and ultra-fine grained zones would soften to varying degrees. Compared with the coarse grained zones, a large number of CNTs distributed in the ultra-fine grained zones weakened its softening effect, and the deformation was more concentrated in the coarse grained zones, therefore, the length/width ratio of the coarse grained zone was large.

The evolutions of sub-structure, CNT distribution and grain structure for the bimodal composites could be described as follows. With increasing the temperature and decreasing the strain rate, dislocation density in the coarse grained zones reduced, and the ratio of DRX increased. Furthermore, at HTLR, the GBs migrated from the coarse grained zones to the ultra-fine grained zones, which led to the CNT re-agglomeration near the BCFZ and the increased content of coarse grained zones. The grain sizes in the ultra-fine grained zones were not affected by the deformation parameters, which were approximately the same as that of the composite before deformation. This is because that the homogeneously distributed CNTs at the GBs could impede the GB migration.

Both LTHR and HTLR could lead to deformation instability. The instable mechanisms under these two parameters were quite different. The deformation instability at LTHR was attributed to the localized shear induced by intense intragranular deformation and internal crack formation, while the deformation instability at HTLR resulted from the more deformation concentrated at the coarse grained zones, and the micro-pore initiation due to CNT re-agglomeration at the BCFZ.

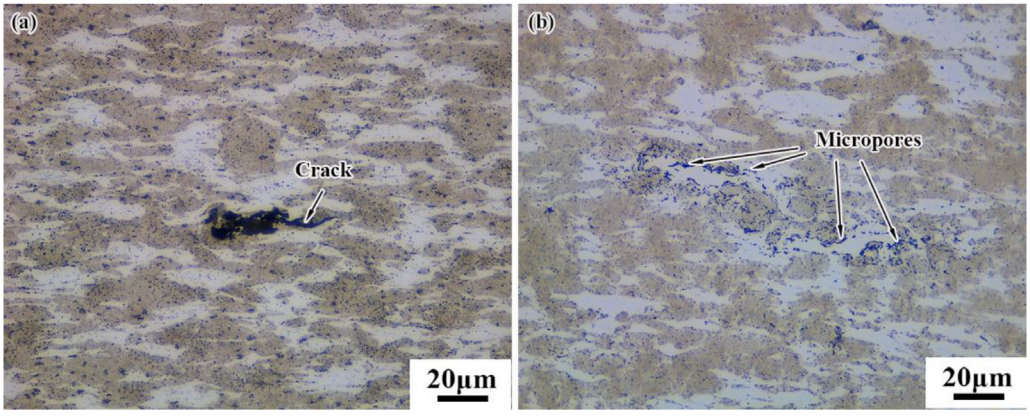

Fig. 9. The damage morphology of bimodal CNT/2009Al composite specimens compressed at (a) 300 °C with 1 s^{-1}, (b) 450 °C with 0.001 s^{-1}.

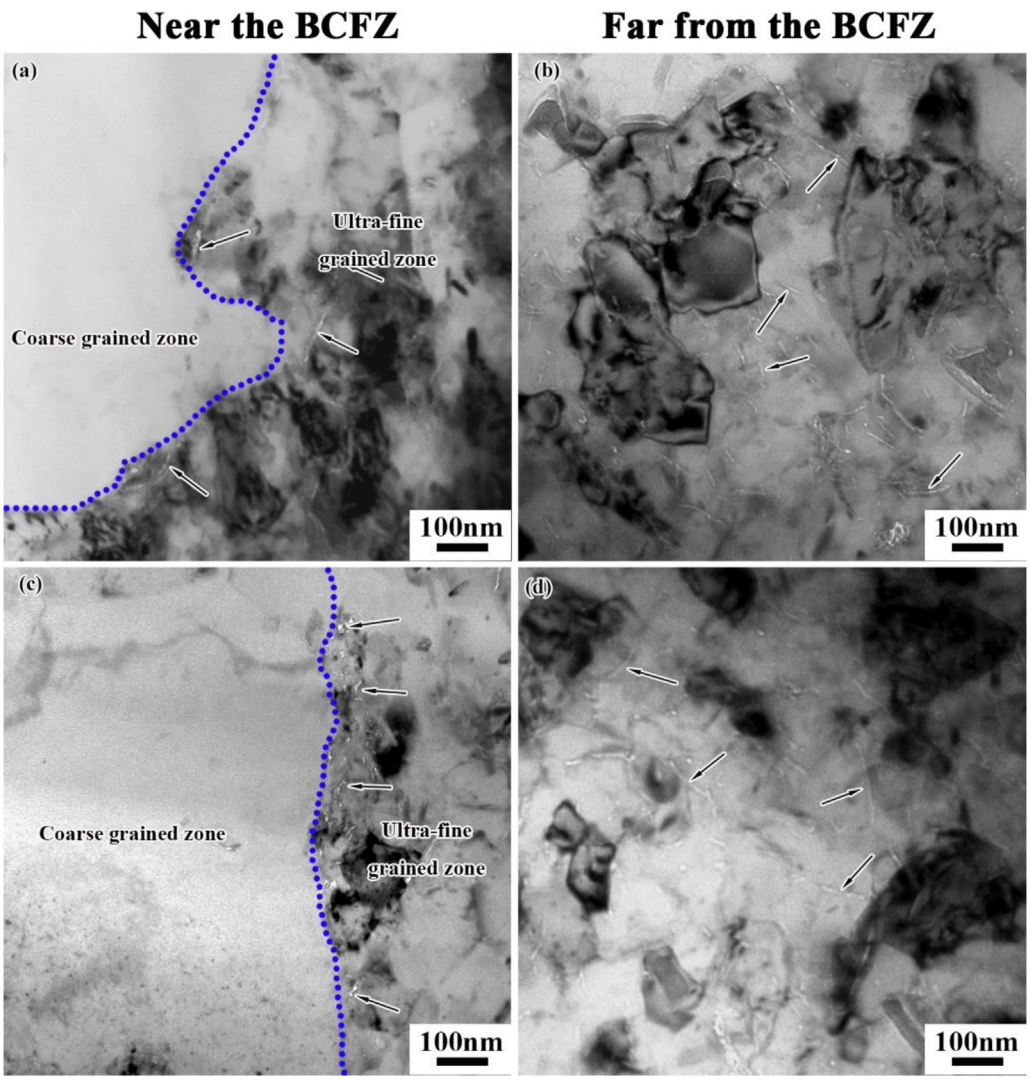

Fig. 10. The CNT distribution for the specimens compressed to a true strain of 0.8 at (a), (b) 300 °C with 1 s^{-1}, (c) (d) 450 °C with 0.001 s^{-1}.

5. Conclusions

In this study, the isothermal compression tests were employed to investigate the hot deformation behavior of the bimodal CNT/2009Al composite at temperatures ranging from 300 to 500 °C with strain rates ranging from 0.001 to 1 s^{-1}. The following conclusions can be drawn as:

(1) The average grain size in the ultra-fine grained zones was basically not affected by the deformation parameters, which was approximately equal to that before hot deformation.
(2) The coarse grained zones were elongated and their long axis directions tended to be perpendicular to the compression direction. Low temperature with high strain rate (LTHR) and high temperature with low strain rate (HTLR) could increase the length/width ratio of the coarse grained zones.
(3) Both LTHR and HTLR could lead to deformation instability. The deformation instability at LTHR was attributed to the localized shear induced by intense intragranular deformation, while the deformation instability at HTLR resulted from the more deformation concentrated at the coarse grained zones, and the micro-pore initiation due to CNT re-agglomeration at the boundaries between the coarse and ultra-fine grained zones during deformation.

Acknowledgments

This work was financially supported by the National Key R&D Program of China (No. 2017YFB0703104), the Key Research Program of Frontier Sciences, CAS (No. QYZDJ-SSW-JSC015), the project of manned spaceflight (No. 040103), the National Natural Science Foundation of China (Nos. 51931009, 51871214 and 51871215) and the Youth Innovation Promotion Association CAS (No. 2020197).

References

[1] S.C. Tjong, Mater. Sci. Eng. R: Rep. 74 (2013) 281–350.
[2] M. Trojanowicz, TrAC-Trends Anal. Chem. 25 (2006) 480–489.
[3] Z. Yu, Z. Tan, G. Fan, D.-B. Xiong, Q. Guo, R. Lin, L. Hu, Z. Li, D. Zhang, Mater. Charact. 137 (2018) 84–90.
[4] R. Xu, Z.Q. Tan, G.L. Fan, G. Ji, D.B. Xiong, Q. Guo, Y.S. Su, Z.Q. Li, D. Zhang, Compos. Part A-Appl. Sci. Manuf. 111 (2018) 1–11.
[5] Z.Y. Liu, K. Zhao, B.L. Xiao, W.G. Wang, Z.Y. Ma, Mater. Des. 97 (2016) 424–430.
[6] X. Yang, T. Zou, C. Shi, E. Liu, C. He, N. Zhao, Mater. Sci. Eng. A 660 (2016) 11–18.
[7] S.E. Shin, D.H. Bae, Compos. Part B-Eng. 134 (2018) 61–68.
[8] K. Zhao, Z.Y. Liu, B.L. Xiao, D.R. Ni, Z.Y. Ma, Acta Metall. Sin. (Engl. Lett.) 31 (2) (2018) 134–142.
[9] Z.Y. Liu, B.L. Xiao, W.G. Wang, Z.Y. Ma, J. Mater. Sci. Technol. 30 (7) (2014) 649–655.
[10] B.K. Choi, G.H. Yoon, S. Lee, Compos. Part B-Eng. 91 (2016) 119–125.

[11] F. Mokdad, D.L. Chen, Z.Y. Liu, D.R. Ni, B.L. Xiao, Z.Y. Ma, Mater. Sci. Eng. A 695 (2017) 322–331.
[12] Z.Y. Liu, B.L. Xiao, W.G. Wang, Z.Y. Ma, Compos. Part A-Appl. Sci. Manuf. 94 (2017) 189–198.
[13] G. Fan, H. Huang, Z. Tan, D. Xiong, Q. Guo, M. Naito, Z. Li, D. Zhang, Mater. Sci. Eng. A 708 (2017) 537–543.
[14] Y.L. Li, M.Y. Shen, H.S. Su, C.L. Chiang, M.C. Yip, J. Nanomater. 2012 (2012) 1–6.
[15] M. Zha, H.M. Zhang, Z.Y. Yu, X.H. Zhang, X.T. Meng, H.Y. Wang, Q.C. Jiang, J. Mater, Sci. Technol. 34 (2) (2018) 257–264.
[16] A.M.K. Esawi, N.T. Aboulkhair, Mater. Des. 83 (2015) 493–498.
[17] Z.Y. Liu, K. Ma, G.H. Fan, K. Zhao, J.F. Zhang, B.L. Xiao, Z.Y. Ma, Carbon 157 (2020) 602–613.
[18] Y.N. Zan, Y.T. Zhou, Z.Y. Liu, G.N. Ma, D. Wang, Q.Z. Wang, W.G. Wang, B.L. Xiao, Z.Y. Ma, Mater. Des. 166 (2019) 8.
[19] X.X. Zhang, J.F. Zhang, Z.Y. Liu, W.M. Gan, M. Hofmann, H. Andrä, B.L. Xiao, Z.Y. Ma, J. Mater. Sci. Technol. 54 (2020) 58–68.
[20] C. Li, R. Qiu, B. Luan, Z. Li, Mater. Sci. Eng. A 704 (2017) 38–44.
[21] Y.N. Zan, Y.T. Zhou, H. Zhao, Z.Y. Liu, Q.Z. Wang, D. Wang, W.G. Wang, B.L. Xiao, Z.Y. Ma,Compos. Part B-Eng. 183 (2020), 107674.
[22] M.M.E.-S. Seleman, M.M.Z. Ahmed, S. Ataya, J. Mater. Sci. Technol. 34 (9) (2018) 1580–1591.
[23] F.P.E. Dunne, Int. J. Plast. 14 (4) (1998) 413–433.
[24] A. Raja, P. Biswas, V. Pancholi, Mater. Sci. Eng. A 725 (2018) 492–502.
[25] S. Pradeep, V. Pancholi, Mater. Sci. Eng. A 561 (2013) 78–87.
[26] C. Xu, G.H. Fan, T. Nakata, X. Liang, Y.Q. Chi, X.G. Qiao, G.J. Cao, T.T. Zhang, M. Huang, K.S. Miao, M.Y. Zheng, S. Kamado, H.L. Xie, Metall. Mater. Trans. A 49 (5) (2018) 1931–1947.
[27] F. Liu, J. Chen, J. Dong, M. Zhang, Z. Yao, Mater. Sci. Eng. A 651 (2016) 102–115.
[28] D.D. Phuong, P.V. Trinh, N.V. An, N.V. Luan, P.N. Minh, R.K. Khisamov, K.S. Nazarov, L.R. Zubairov, R.R. Mulyukov, A.A. Nazarov, J. Alloys Compd. 613 (2014) 68–73.
[29] F. Mokdad, D.L. Chen, Z.Y. Liu, D.R. Ni, B.L. Xiao, Z.Y. Ma, Mater. Sci. Eng. A 702 (2017) 425–437.
[30] H. Mirzadeh, J.M. Cabrera, A. Najafizadeh, P.R. Calvillo, Mater. Sci. Eng. A 538 (2012) 236–245.
[31] Q. Yang, Z. Deng, Z. Zhang, Q. Liu, Z. Jia, G. Huang, Mater. Sci. Eng. A 662 (2016) 204–213.
[32] Z. Huang, X. Zhang, B. Xiao, Z. Ma, J. Alloys Compd. 722 (2017) 145–157.
[33] E.A. El-Danaf, A.A. Almajid, M.S. Soliman, J. Mater. Eng. Perform. 17 (2008) 572–579.
[34] C. Shi, X.G. Chen, Mater. Sci. Eng. A 650 (2016) 197–209.
[35] A.A. Khamei, K. Dehghani, R. Mahmudi, JOM 67 (2015) 966–972.
[36] C.H. Li, R.S. Qiu, B.F. Luan, W.J. He, Z.Q. Li, Trans. Nonferrous Met. Soc. China 28 (2018) 1695–1704.
[37] B.L. Xiao, Z.Y. Huang, K. Ma, X.X. Zhang, Z.Y. Ma, Acta Metall. Sin. 55 (2019) 59–72 (in Chinese).
[38] X. Li, C. Liu, X. Sun, M. Ma, R. Liu, Sci. China-Technol. Sci. 59 (2016) 980–988.
[39] S. Murty, B.N. Rao, J. Phys. D-Appl. Phys. 31 (1998) 3306–3311.
[40] Y. Prasad, Indian J. Technol. 28 (1990) 435–451.
[41] W.J. He, C.H. Li, B.F. Luan, R.S. Qiu, K. Wang, Z.Q. Li, Q. Liu, Nonferrous Met. Soc. China 25 (2015) 3578–3584.
[42] A. Esawi, K. Morsi, Compos. Part A-Appl. Sci. Manuf. 38 (2) (2007) 646–650.
[43] Z.C. Sun, H.L. Wu, J. Cao, Z.K. Yin, Int. J. Plast. 106 (2018) 73–87.
[44] J. Zuo, L. Hou, J. Shi, H. Cui, L. Zhuang, J. Zhang, Mater. Charact. 130 (2017) 123–134.
[45] Y.C. Lin, L.T. Li, Y.C. Xia, Y.Q. Jiang, J. Alloys Compd. 550 (2013) 438–445.
[46] M.F. Ashby, Surf. Sci. 31 (1972) 498–542.
[47] T.G. Nieh, J. Wadsworth, T. Imai, Scr. Mater. 26 (5) (1992) 703–708.
[48] H.Y. Kim, S.H. Hong, Scr. Mater. 30 (3) (1994) 297–302.
[49] X. Kai, C. Chen, X. Sun, C. Wang, Y. Zhao, Mater. Des. 90 (2016) 1151–1158.
[50] M. Rajamuthamilselvan, S. Ramanathan, Mater. Manuf. Process 27 (2012) 260–266.
[51] V. Senthilkumar, A. Balaji, R. Narayanasamy, Mater. Des. 37 (2012) 102–110.